Multiple-resonant pad-rod nanoantennas for surface-enhanced infrared absorption spectroscopy

DOI:
10.1088/1361-6528/ab3b69

Document Version
Accepted author manuscript

Multiple-resonant Pad-rod Nanoantennas for Surface-Enhanced Infrared Absorption Spectroscopy

Weisheng Yue[1], Vasyl Kravets[2], Mingbo Pu[1], Changtao Wang[1] and Zeyu Zhao[1] and Zhirun Hu[3,4]

[1]State Key Laboratory of Optical Technologies on Nano-Fabrication and Micro-Engineering, Institute of Optics and Electronics, Chinese Academy of Sciences, P.O. Box 350, Chengdu 610209, China

[2]School of Physics and Astronomy, University of Manchester, Oxford Road, Manchester M13 9PL, United Kingdom

[3]School of Electrical and Electronic Engineering, University of Manchester, Sackville Street, Manchester M13 9PL, United Kingdom

[4]National Graphene Institute, Oxford Road, Manchester M13 9PL, United Kingdom

Abstract

Due to the ability to tightly confine electromagnetic energy, plasmonic nanoantennas have been widely studied for surface-enhanced infrared absorption (SEIRA) spectroscopy, surface-enhanced Raman spectroscopy (SERS) as well as refractive-index sensing. However, most of the nanoantennas are limited by narrow resonant band and it is rather challenging to detect multiple molecular fingerprints. In this work, we report dual and triple- resonant pad-rod plasmonic nanoantennas which are nanorods with large pads at theirs placed above gold (Au) mirror separated by a spacer layer. By adjusting the geometries, the nanoantennas have demonstrated dual and triple resonant bands enabling detection of molecular fingerprints at different wavelength. The calculated maximum SEIRA enhancement factor is around 1.8×10^{6},

which is among the highest reported so far. The pad-rod plasmonic nanoantennas have been used for the detection of molecules of PMMA (polymethyl methacrylate) by SEIRA and fingerprints of C=O and C–H bands are clearly identified. This work has shown that the multiple-resonant pad-rod plasmonic nanoantennas are promising for chemical and biomolecular sensing by the detection of vibrational fingerprints with SEIRA.

1. Introduction

Plasmonic nanoantennas continue to attract a great deal of interests due to their capability of confining free-space electromagnetic (EM) waves into subwavelength regions with high field enhancement. Strong local EM fields produced on the surface of plasmonic nanoantennas have enabled a variety of applications such as SERS, SEIRA, biochemical sensing, medical diagnostic and so on [1]. There are large amount of works reported on the SERS enhancement by various types of antennas [2-4]. However, SEIRA with plasmonic nanoantennas are well less reported due to much smaller IR absorption cross-section of molecules and thus SEIRA is more challenging than SERS. Infrared absorption spectroscopy is an important analytical technique that complements Raman spectroscopy to acquire molecular vibrational fingerprints in a label-free manner [5]. Thus, there is a substantial motivation to enhance SEIRA to single-molecule or few-molecule sensitivity by investigating suitable plasmonic nanoantennas with a large field enhancement.

Majority of research efforts have been focused on optimizing the design of the size, shape and arrangement of plasmonic nanostructures. Different kinds of geometrical shapes like nanodisc, nanospheres, nanoholes, and U-shaped split ring resonators have been designed and investigated [6-8]. In addition to standard noble metals like Au and Ag, germanium, Si, aluminum as well as graphene have been used for plamsonic nanoanennas [9-13]. Among

various designs, adjacently placed metallic nanoparticles with nanogaps are most favorable in designing plasmonic nanoantennas. Coupling effects occurs between the adjacent nanoparticles or tips and the local fields in the gap can be significantly enhanced. Nanogaps with sub-10 nm can produce extremely high electric field enhancement [14-15]. Further reduction of gap size is difficult due to limitation of fabrication process.

Recently, multi-layered plasmonic nanostructures have demonstrated potential to enhance EM fields by cavity effects in the multi-layers. Typical multilayered plasmonic nanoanennas are MIM structures by which the incident light can be confined in the form of surface plasmon polaritons (SPPs) propagated along the surface of metallic film [17-19]. The MIM plasmonic structures can achieve high field enhancement and optical response by the cavity effects; partially circumvented the difficulties in fabrication of extremely fine and precision nanostructures. In addition, the optical response can be tuned by adjust the thickness of the spacer layer, which cannot be achieved by the in-plane nanostructures. Liu *et al.* reported MIM disc plasmonic nanoantennas as sensors for different liquid materials [20]. Bhattarai *et al.* reported that MIM mushroom-capped plasmonc absorber can increase the sensitivity in refractive sensing [21]. Although these methods are efficient in various sensing applications, they are limited by working wavelength range due to the narrow resonance band. When one wants to indentify more molecular fingerprints simultaneously, dual or multiple-resonant plasmonic nanoantnenas will be desirable. Dual or multiple-resonant plasmonic nanoantennas have been reported and applied to SERS and SEIRA enhancement for different molecular fingerprints [22-24]. However, these nanoantennas are mostly lack of nanogaps and the sensitivity is limited. Recently, combination of large pad and small rods (pad-rod) are introduced in designing plasmonic nanoantennas. In these kind of geometries, the large pad works like charge reservoir to provide larger field enhancement. Brown *et al.* reported such kind of pad-rod nanoantennas with fan pad and Dong *et al.* developed bowtie-shaped

nanoantennas with large pads to improve SEIRA sensitivity [25, 26]. The drawback of the reported work is that the absorption only occurs at single wavelength where the resonance was excited. In addition, the field enhancement can be further improved to achieve higher sensing sensitivity.

In this work, pad-rod nanoantennas with dual and triple resonances in infrared ranges are investigated for their optical prosperities SEIRA sensing capability. The pad-rod nanoantennas consist of a pair of nanorods with large pad at ends, to work as electric resonators on top of Au mirror which is separated by Al_2O_3 spacer layer. Dual and triple resonances are achieved by optimizing the thickness of spacer and the geometries of resonators. To demonstrate the sensing capability, 50 nm-thick polymerthyl meethacrylate (PMMA) film molecules were tested. C=O and C-H bands of the film were clearly detected. In comparison with previously reported antennas, the pad-rod antennas in this work have advantages of multiple resonances and higher field enhancement. This work provides impetus on many fields of nanoscience and will foster various applications in high-impact areas such as metamaterials, light harvesting, and sensing or the fabrication of nanophotonic devices.

2. Experiments

2. 1 Fabrication process

The arrays of the pad-rod nanoantennas were fabricated with electron beam lithography in combination with lift-off process. Figure 1 shows the fabrication procedures: (1) Cleaned silicon substrate was sequentially deposited with 3 nm thick titanium (Ti) film, 100 nm Au film and 170 nm Al_2O_3 film. The Ti layer serves adhesion layer between the Si and Au and the Au layer works as ground plane. The spacer layer Al_2O_3 was deposited by means of atomic layer deposition (ALD). (2) PMMA (950 A3) resist was spin-coated onto the Al_2O_3 surface to a thickness of 150 nm. (3) Arrays of pad-rod nanoanennas were exposed in PMMA using electron beam lithography (Raith EBPG 5200). (4) After development of the pattern,

Ti/Au layer with thickness of 3 nm and 60 nm, respectively, were evaporated on the surface. (5) The final plasmonic antennas were obtained using lift-off procedure and resist removed with acetone.

Figure 2 shows SEM images of the fabricated fan pad-rod and rectangle pad-rod nanoantennas. The geometrical shapes were well controlled with the high resolution electron-beam lithography technique.

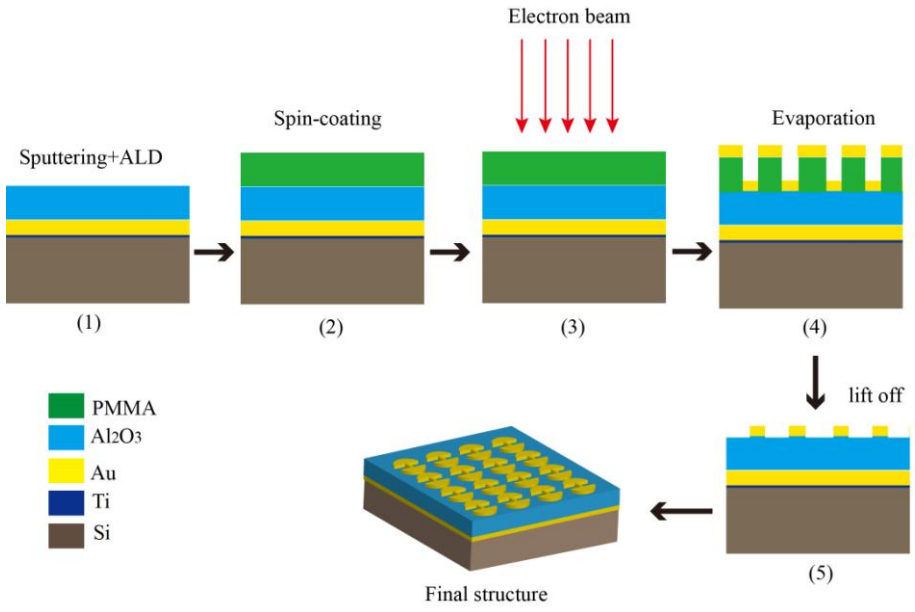

Figure 1. Fabrication procedure of pad-rod plasmonic antennas

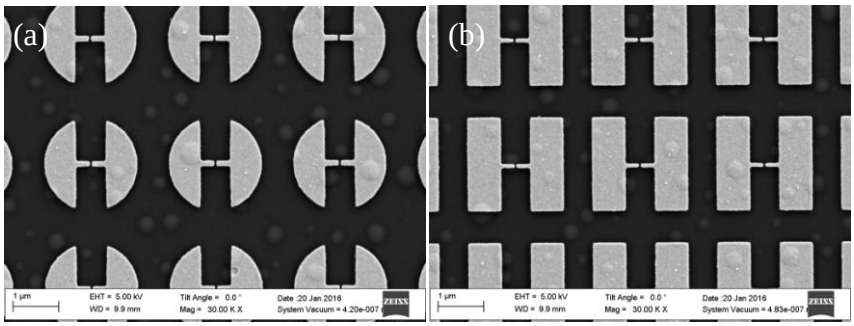

Figure 2. SEM images of fabricated fan pad-rod(a) and rectangle pad-rod (b) nanoantennas.

The optical measurements of the nanoantennas were performed by a Fourier Transform IR spectrometer coupled to an IR microscope (Bruker Vertex 80V and Hyperion 3000). The

polarization of the incident IR was polarized along the gap direction (X-direction, Px) to take advantage of the gap effect. Reflection spectra were collected through a Swcharzchild objective and measured by a liquid-nitrogen-cooled mercury-cadmium-tellurium (MCT) detector. The measured reflection spectra are normalized to the spectra collected at blank areas without the patterns.

2.2. Numerical simulations

The numerical simulations of the nanoantennas were performed with commercial software CST Microwave Studio [27], based on finite integration technique (FIT). A frequency-domain solver was used with unit-cell boundary conditions in X-Y plane and floquet ports were applied in the Z direction. In the simulations, the dispersion properties of the of Au was modelled as Drude dielectric function,

$$\varepsilon(\omega) = \varepsilon_{\infty} - \frac{\omega_p^2}{\omega^2 + i\omega\gamma},$$

where ε_{∞}=9.1 is the high-frequency limit dielectric constant. The plassmon frequency of Au ω_p=1.3659×10^{16} rad/s and damping frequency of γ =1.0738×10^{14} rad/s are taken from [20, 28].

3. Results and Discussion

3.1 Principle and design

Two types of pad-rod nanoantennas were studied and designed: one is fan (semi disc) pad and the other is rectangle pad. Figure 3 shows schematics of the nanoantennas with nanorod and fan-shaped pad and rectangle-shaped pad. Figure 3(a) is perspective view of the pad-rod nanoantennas. Figure 3(b) and (d) are top view of the fan pad-rod and rectangle pad-rod antennas, respectively. Figure 3(c) is side view of the nanoantenna. The thickness of the top layer metal, Al_2O_3 spacer, and the reflective Au film is 60, 170, and 100 nm, respectively. In

the pad-rod nanoantennas, the large pads work as charge reservoirs and squeeze charges the rod end, resulting in a higher localized EM fields at the tips. The closely placed tips promote the coupling of the LSPR (local surface plasmon resonance) at the adjacent two faced tips.

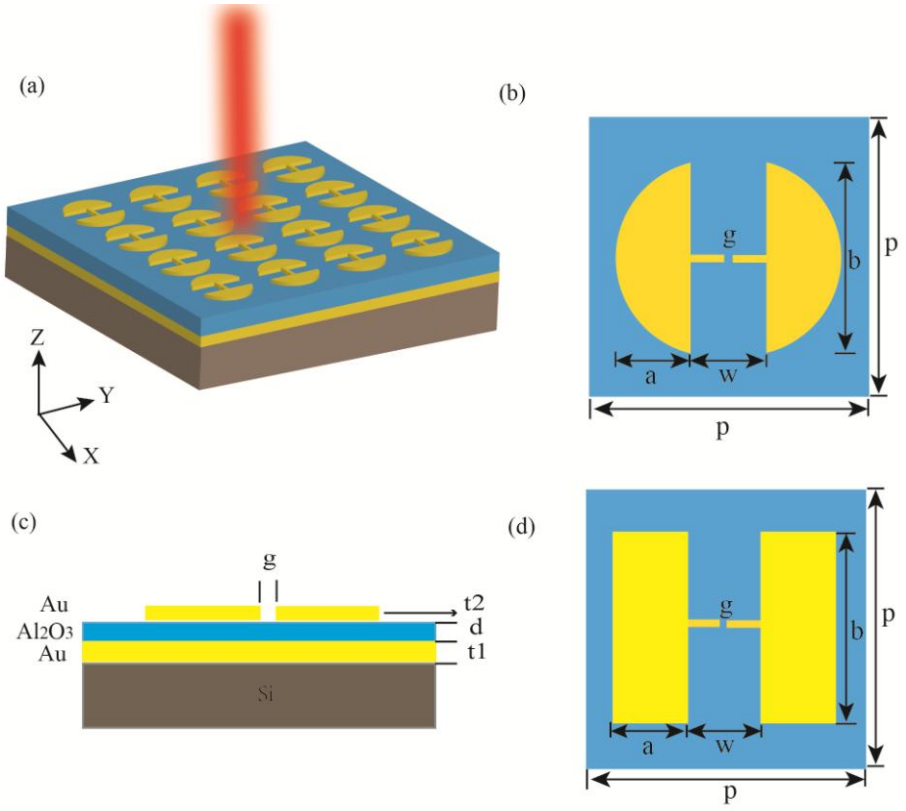

Figure 3. Schematic of pad-rod plasmonic nanoantennas. (a) Array of fan pad-rod nanoantenna, (b) top view of fan pad-rod nanoantenna, (c) side view of pad-rod nanoantenna, (d) top view of rectangle-pad nanoantenna. Dimensions in the schematic are a=700, b=2100, w=665, p=2000, t1=100, t2=60, d=170. Tip width is 70 nm and the gap g is variable from 0, 30, 40, 50 to 60 nm.

To demonstrate the working principle of the MIM pad-rod nanoantennas, we simulated electromagnetic proprieties and optical reflection spectra of nanorods and fan pads, respectively. Figure 4(a) shows the simulated EM field distribution of individual nanorods. The two nanorods form a small gap in between and they are placed on Al_2O_3 film which separates them from bottom Au layer. The upper part in figure 4(a) exhibits simulated electric field distribution on the nanoantennas and the lower part displays the induced surface current

density. It can be seen from the electric field distribution that each nanorod works as a dipolar resonator under excitation of incident EM wave with polarization along the bar. High field is at the end of each nanorod and the field in the gap region is strengthened due to the field coupling effects between the tips. Charging by the plasmon oscillations results in anti-phase oscillation of a mirror plasmon in relation to that in the ground Au film. Consequently, a circular current distribution accompanied by a magnetic response is totally located within the MIM system. At certain frequencies, the wave energy can be coupled into MIM system through resonance, which leads to a nearly completed absorption of incident light. Figure 4 (a2) shows the simulated reflectance of the nanobar dimer, which demonstrates a high absorption and sharp band at the resonant frequency f=67 THz. Figure 4(b) is the simulated electric field distribution and reflectance spectra of the fan pads. Similar reflectance spectra with the pair of nanorods are observed due to the MIM configuration. However, the resonance frequency is higher due to that the size in the excitation direction is smaller than that of the nanorods. The electric field distribution also shows the dipolar resonance mode in the X-direction. Figure 4(c) shows electric distribution (c1) and reflection spectrum of fan pad-rod antenna. It exhibits the features for the both nanorods and pads. Two absorption dips occurs at the reflection spectrum, which is the combination of from the absorption of the nanorod and the fan pads. With the combination of nanorods and pads, the field intensity at the gap area is further enhanced due to the squeezing effects of the charges from pads to the nanorods. Reflective substrate is effectively in enhancing local EM fields.

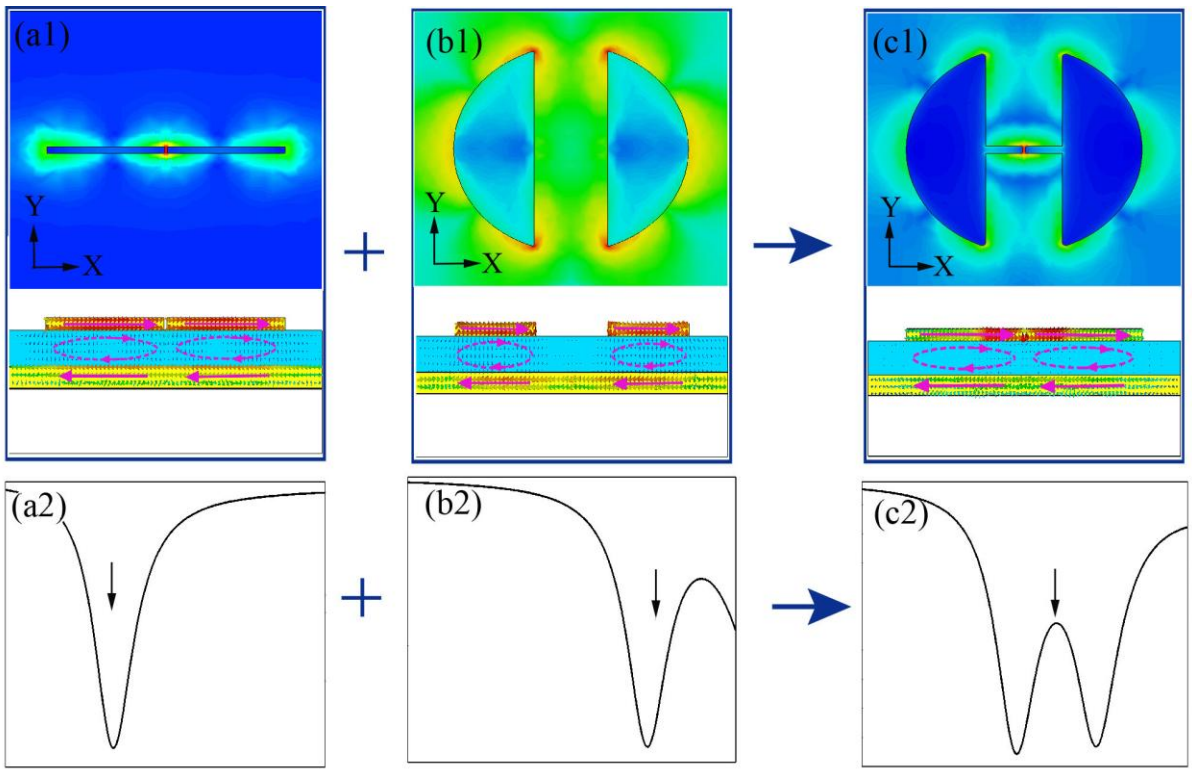

Figure 4. Operational principle of the pad-rod nanoantenna. (a1-c1) are electric field distribution of nanorods, fan pads and fan pad-rod nanoantenna. (a2-c2) are reflection spectra corresponding to the plasmonic nanoantennas (a1-c1). The arrows indicate the field monitoring position.

3.2 Infrared spectroscopic characterization

We first investigated spectra properties of normal fan pad-rod antennas with polarization along gap direction. Dual-band absorption was achieved with the fan pad-rod nanoantennas. Figure 5(a) shows the measured reflectance of the antennas of the fan pad-rod antennas. The fan pad-rod nanoantennas with gap in the middle show dual-band resonant features. The pad-rod antennas without gap in the middle shows only one resonance absorption dip at around 87 THz (black curve). This is caused by the dipolar resonance of each pad. The strong absorption can be ascribed to impedance matching of the MIM

structures [29]. For the other fan pad-rod antennas gaps, they are all featured with two resonance dips with a transparent peak between the two dips. One is at around 76 THz and the other is at around 87 THz. It is clear that the resonance dip at 76 THz is caused by the nanogap. The coupling of LSPR on the tips of the gap causes the strong absorption. This coupling effect is sensitive to the gap size. When the gap sizes increase from 30 to 40, 50 and 60 nm, the resonance shifts from 74, to 76, 78, and to 80 THz, respectively. It is observed that the resonance at the 87 THz are not sensitive to the gap size, the change of gap size doesn't clearly change the resonances. This is because this resonance is caused by the pads. The superposition of two resonances modes at 76 THz and 87 THz results in the EIT-like peaks (electromagnetically induced transparency). With the increase of the gap size, the intensity of the EIT-peaks decreases and the positions shift towards higher frequencies. The EIT is typical nonlinear optical phenomenon and is useful in developing various sensing devices. The fabricated fan pad-rod nanoantenas induced sharp reflectance peak within the broad resonance spectral band (see Figure. 5) which is with analogy of ref.[30] and can be established as EIT-like effect. In abovementioned work, EIT-like effect was experimentally demonstrated in complementary planar metamaterials. Sharp reflectance peaks are observed in pad-rod nanoantenas due to producing sharp and narrow gaps between the pad-rod resonators by using electron beam lithography of ultrahigh resolution. As results of coherently coupled different plasmonic modes a pronounced reflectance peaks are appeared within a broad spectral shape. Figure 5(b) shows the simulated reflection spectrum of the fan pad-rod nanoantennas. The measured results agree very well with the simulated results.

To understand the electric field enhancement at the resonant wavelengths, electric field distributions are simulated with the CST Microwave Studio at the each resonance position for the fan pad-rod nanoantennas with gap of 30 nm. In the simulation, the incident light is normal to the surface and polarized along horizontal direction. The simulated field

distributions are shown in figure 6. Figure 6(a1) and (a2) presents the electric field distribution on the top surface and on the vertical cross-section plane, respectively. The fields correspond to the resonance at 74 THz. It is seen from figure 6(a1) that the local electric field is highly enhanced in the gap areas. From figure 6(b2), it is seen that the reflective mirror effect of the Au film at the bottom is clear in enhancement of the electric field. The maximum field enhancement occurs at the gap regions for the 74THz resonance. The calculated electric field enhancement ($\mathbf{E/E_0}$) in the gap is around 1260, where **E** is the local electric field intensity and $\mathbf{E_0}$ is electric field 2 nm above Si surface without antenna. This field enhancement leads to SEIRA enhancement factor EF of 1.6×10^6, which is estimated with formula $EF \propto \left|\frac{E}{E_0}\right|^2$. This EF is 13 times higher than that reported in [25]. The SEIRA EF is general lower than SERS EFs because the SERS EF is proportional to 4^{th} power of field enhancement.

Figure 6(b1) and (b2) shows the electric field distribution of the fan pad-rod nanoantenna with 30 nm gap at the resonance 85 THz. the distribution model is different from that of the resonance at 74 THz. High electric field is located at the outer edges, the corners and the gap area. Figure 6(b2) shows electric field on the vertical cross-section plane. Our simulation exhibits strong contribution from reflective Au mirror on the summarised field enhancement. Compared to the field distribution of the resonance at 74 THz, the electric field at the resonance at 85 THz is less confined in the gap area, but more uniformly distributes on the surface. This is also useful to increase the sensing area. The field enhancement ($\mathbf{E/E_0}$) in the gap area is around 230, corresponding to to SEIRA enhancement factor EF of 5.3×10^4. This EF is comparable with most of plasmonic nanoantennas for SEIRA but is relative lower than that at the resonance of 74 THz. The above investigation shows that the fan pad-rod nanoantennas can strongly enhance electric field intensity at both

the resonant wavelengths. It is interesting to note that our proposed arrays of fan pad-rod nanoantenna show higher near field enhancement factors than previously reported in [25]. Main difference between our nanostructure and studies in [25] is next: (i) the height of Au fan-shaped nanostructure in our study is larger (60 nm) than used in work [25] (only 35 nm); (ii) the spacer layer was chosen as Al_2O_3 with the optimal optical thickness $n_{Al2O3}*d$, where n_{Al2O3} and d is the refractive index and geometrical thickness of Al_2O_3, less than a quarter of the resonant wavelength. We can assume that the near field intensity is additionally enhanced by constructive interference of scattered electromagnetic waves and strongly depend on large scattering cross-sections of thicker pad-rod nanoantennas.

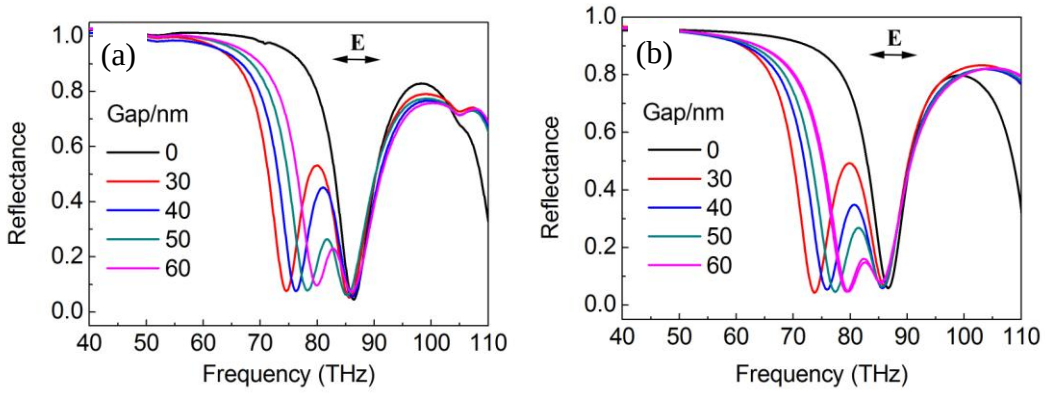

Figure 5. Experimental (a) and simulated (b) reflection spectra of the fan pad-rod nanoantennas with gap 0, 30, 40, 50 and 60 nm. The arrows indicate polarization direction.

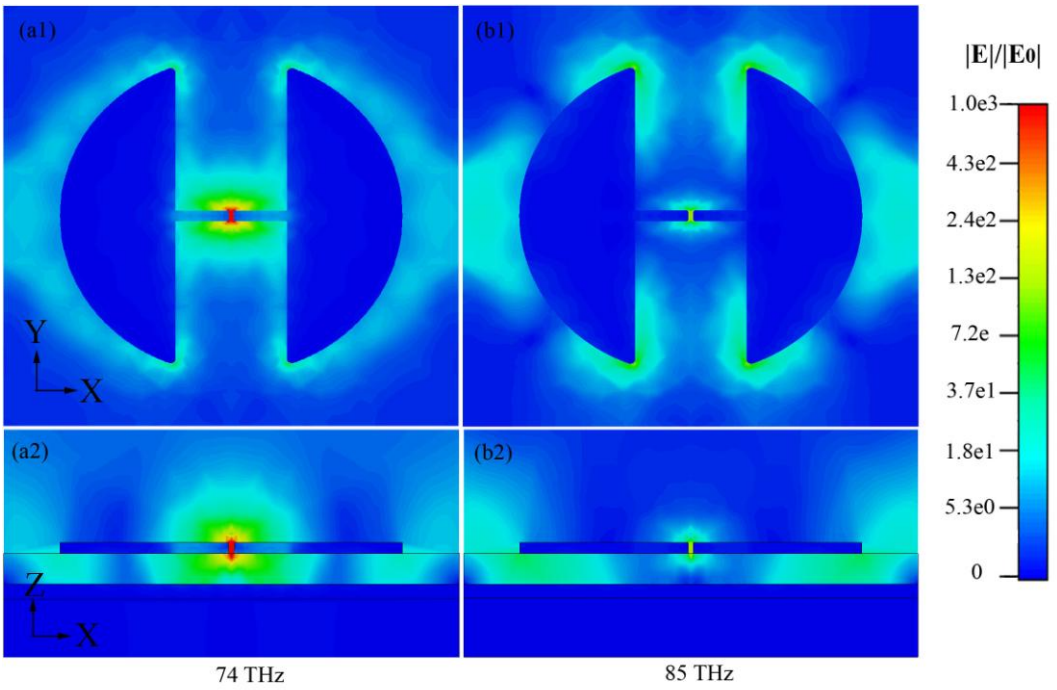

Figure 6. Simulated EM fields of the fan pad-rod nanoantennas with 30 nm gap. (a1, b1) electric field at the top; (a2, b2) electric field at the vertical cross section plane. The intensities are plotted in a logarithmic scale.

When the geometry of the pad was changed to rectangle shape, the pad-rod antennas demonstrated triple-band resonances. Figure 7 presents the experimental (a) and the corresponding simulated (b) reflection spectra of the rectangle pad-rod nanoantennas. The rectangle pad-rod nanoantennas with gaps of 30, 40, 50 and 60 nm were investigated. There are three resonance dips at around 72, 82 and 99 THz. The resonance at the 72 THz is formed by the coupling of EM fields from the two tips connected to the pads, which have the similar physical origin as that that of the 74 THz resonance mode in the case of the fan pad-rod nanoantenna. This resonance is sensitive to gap size. With the increase of the gaps, the resonance dip shift to higher frequencies. This dependence can be understood with a *LC* (inductor-capacitor) circuit mode. The two face-to-face apexes form a capacitor in the *LC* circuit. With the increase of the gap, the capacity decreases, resulting in the increase of

resonance frequency according to $\omega \propto 1/\sqrt{LC}$. The resonance mode at 84 THz and 99 THz can be ascribed to splitting of the resonance at around 87 THz. It was shown that the tiny gap between the nanorods renders possible an effective near-field coupling between the rods that leads to the splitting of the single rod resonance into two hybrid dimer modes (called bonding and antibonding ones) [31].The band at 84 THz is insensitive to the gap size. The change of gap size did significantly change the resonance position. The resonance mode at 99 THz has a broader absorption band which is due to the large size of the pad. The rectangle pad-rod antennas have three resonances while the fan pad-rod antennas have two resonances. This is because their difference in geometrical shape. The rectangle pad-rod antennas have larger interaction areas than that of the fan pad rod antennas. The gathering light from hollow cone (not only normal incidence) is demonstrated to be the important feature that enables the excitation of the bonding resonance of the structure using far-field illumination. It is possible reason that tiny rectangle pad-rod antenna features three resonances whereas the fan pad-rod antenna only features two. Reflection spectra of the rectangle-pad antenna without gap (g=0) are shown in black curve. The multiple resonance modes are flexible in redetection of molecules of different fingerprints in SEIRA.

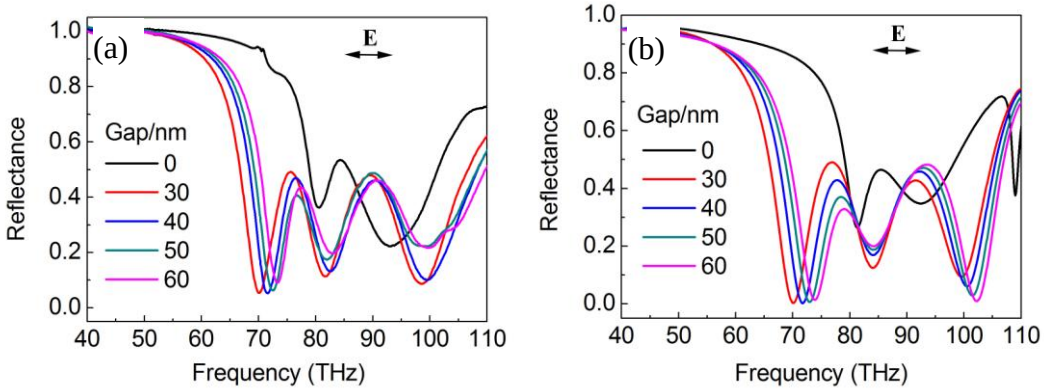

Figure 7. Experimental (a) and simulated (b) reflection spectra of the rectangle pad-rod nanoantennas with gap 0, 30, 40, 50 and 60 nm. The polarization of incident light is along the gap direction.

Electric field distributions for the each resonance dips in the case of the rectangle-pad nanoantenna with 30 nm gap were simulated and presented in figure 8. Figure 8(a1, a2) shows the electric and magnetic field distribution on the top and on the vertical cross-section plane at the resonance dip 70 THz. In figure 8(a1), the electric field is highly confined in the gap region while weak field intensity at the pad edges, indicating the coupling of LSPR between the two nanoantennas tips. In figure 8(a2), high field at the gap region is radiated to air and the dielectric space layer. Again the contribution of reflection from the Au mirror at the bottom is obvious. Figure 8(b1, b2) are electric field distribution at the band 84 THz. In figure 8(b1), high electric field intensity distributed at the outer middle edges and the inner corners, showing a triangular distribution mode. The intensity in the gap region was slightly less confined in comparison with that in figure 8(a1). In Figure 8(b2), high field is observed at the both ends of the pad and the gap region. Figure 8(c1, c2) illustrate electric field distribution for the band 99 THz. This mode corresponds to the dipolar resonance of the pads. High electric field is at the gap region. On the pads, the electric field is symmetrically distributed, indicating dipolar resonance mode. Electric field enhancements ($\mathbf{E/E_0}$) in the gap region are calculated at the resonance 70, 84 and 99 THz. They are around 1360, 650 and 940, respectively. The field enhancements lead to SEIRA enhancement factor EF of 1.8×10^6, 4.2×10^5 and 8.8×10^5. These EFs are among the highest level of the reported. The reported SEIRA EFs are generally on the order of 10^5. The investigation indicated that the rectangle pad-rod nanoantenna have advantages of electric field enhancement. The electric field intensity is highly enhanced at all the three resonant bands. These features are very promising in enhance the detection sensitivity of multiple molecular fingerprints.

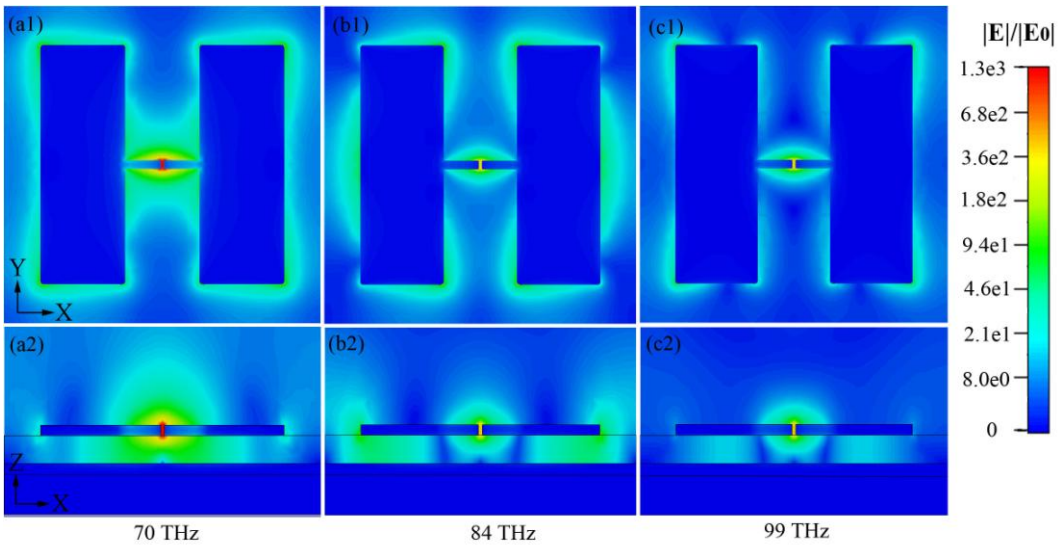

Figure 8. Simulated EM field distribution for the rectangle pad-rod with 30 nm gap. (a1-c1) electric field at the top of the structured surface; (a2-c2) electric field distribution on vertical cross section plane. The intensities are plotted in a logarithmic scale.

4. Surface-enhanced Infrared Spectroscopy of PMMA molecules

A strong field enhancement in infrared spectra region promises a sensitive sensing platform. As a proof of concept, infrared spectroscopy measurements of PMMA molecules on the plasmonic nanoantennas were performed. PMMA polymer is used because it has several well-characterized absorption bands in the infrared range. In the measurements, PMMA resist was spin-coated on the surface of pad-rod nanoantennas to a thickness of ~50 nm. After spin-coating, the substrate was baked for 10 min on hot plate at 150 ˚C to evaporate the solvent. Measurements were performed with the same FTIR spectrometer as used above. The reflection spectra of the PMMA coated nanoantenna are shown in figure 9. Several molecular fingerprints of the PMMA molecules have been detected by the plasmonic nanoantennas. Figure 9(a) presents the measured SEIRA spectra with the fan pad-rod antennas. The absorption feature at 1732 cm^{-1} shows the presence of acrylate carboxyl group

(C=O) in PMMA. The absorption differences are 14.5%, 13%, 13%, 11.4% for the fan pa-rod antennas with gaps of 30, 40, 50 and 60 nm. The antennas without gap (gap 0) cause a minimum absorption difference 8%. The features at 2997 cm^{-1} can be assigned to C-H bond stretching vibrations (2955 cm^{-1}, 2989 cm^{-1}). The absorption differences of the C-H bond are around 2%. The intensity of the C=O bond is larger because of its intrinsic large dipole moment and the interaction between the molecular dipole moment with the plasmonic mode of the nanoantennas. The dipole moments of C-H stretches are small and they are not easily to be measured. However, they are clearly detected in our in our proposed nanoantennas, suggesting that our proposed plasmonic nanoantennas are well suitable for molecular vibrational spectroscopy. Figure 9(b) is the SEIRA measurements of the PMMA with the rectangle pad-rod. Similarly, the two bands of the vibration modes of PMMA, C=O and C-H, are clearly detected. To verify the enhancement effect, we measured FTIR spectra of PMMA with the same thickness deposited on pure silicon wafer using the same experimental conditions. As is expected, no clear absorption peaks are determined. Although the C=O and C-H bands are clearly detected with the two types of plasmonic antennas, it should be noted that the molecular fingerprint frequencies are on the slope of the infrared absorption dips of the plasmonic antennas. We can assume that the detection sensitivities can be further improved by tuning the plasmonic resonances to that of the molecular fingerprints.

To quantitatively evaluate the enhancement effect of the pad-rod antennas, the SEIRA enhancement factors (EFs) were calculated by equitation $EF = (\Delta R_{SEIRA}/D_{SEIRA})/(\Delta R_{ref}/D_{ref})$ [32, 33], where ΔR_{SEIRA} and ΔR_{ref} is the difference of the SEIRA and reference IR dip in the reflection spectrum between the maximum and the minimum value at each vibrational wavelength, respectively. D_{SEIRA} and D_{ref} is the thickness of the film on the pad-tip antennas and the reference film, respectively. To evaluate the EF, the infrared absorption spectra of an 830 nm thick reference film of PMMA on bare Si surface were measured. The EF values of

PMMA on the fan and rectangle pad-tip antennas were listed in table 1. The EFs of the C=O bond are 170-220 on the fan pad-rod antennas with gap and 250-270 on the rectangle pad-rod antennas with gap. The EFs of the C-H mode are around 220 on the fan pad-rod antennas with gap and around 100 on the rectangle pad-rod antennas with gap. Due to the flat resonance line shape, the EFs of the C-H bond are smaller on the rectangle pad-rod antennas than that on the fan pad-rod antennas. It is noted that the experimental EFs are much lower than the calculated EFs according to the field enhancement. This is because the mismatching of the antennas resonances with molecular vibrational modes, suggesting us to improve the experimental EFs to the numerically calculated EFs by optimizing the resonances to overlap the molecular absorption frequencies of vibrational modes.

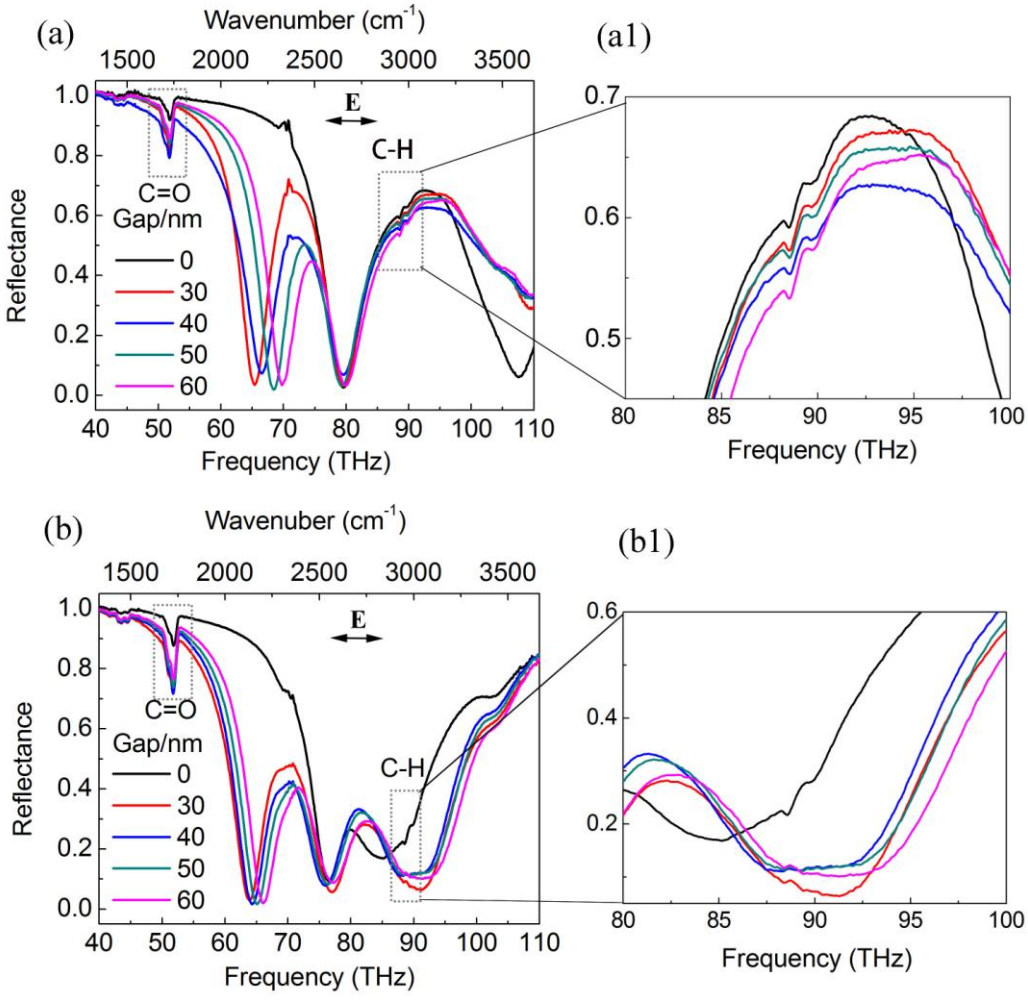

Figure 9. SEIRA spectroscopy of PMMA deposited on the pad-tip nanoantennas. (a) PMMA on the fan pad-tip antenna.(b) PMMA on the rectangle pad-rod antenna. (a1) and (b1) are the magnification of the indication vibrational modes indicated by dotted rectangle in (a) and (b).

Table 1 Calculated experimental SEIRA EFs of PMMA vibrational modes at the fan and rectangle pad-rod antennas.

Gap(nm)	Enhancement factors			
	C=O		C-H	
	Fan	Rectangle	Fan	Rectangle
30	219	267	228	208
40	196	297	228	93
50	198	281	218	104
60	172	254	218	145
0	121	140	208	208

The SEIRA of PMMA with Y-polarized incident light was investigated and presented in figure 10. For the fan pad-rod antennas, we have observed similar C=O and C-H absorption. The absorption difference of the C-H bond is less significant in comparison with that with the X-polarized excitation (see figure 9a), indicating the advantages of the gap in the SEIRA enhancement. For the rectangle pad-rod antennas, the absorption of the C=O bond is stronger than that with the X-polarized excitation shown in 9b. This is because the good spectral overlap of the vibration band with the resonance. The absorption of the C-H bond is clear with is similar to that of the SEIRA with the X-polarized light.

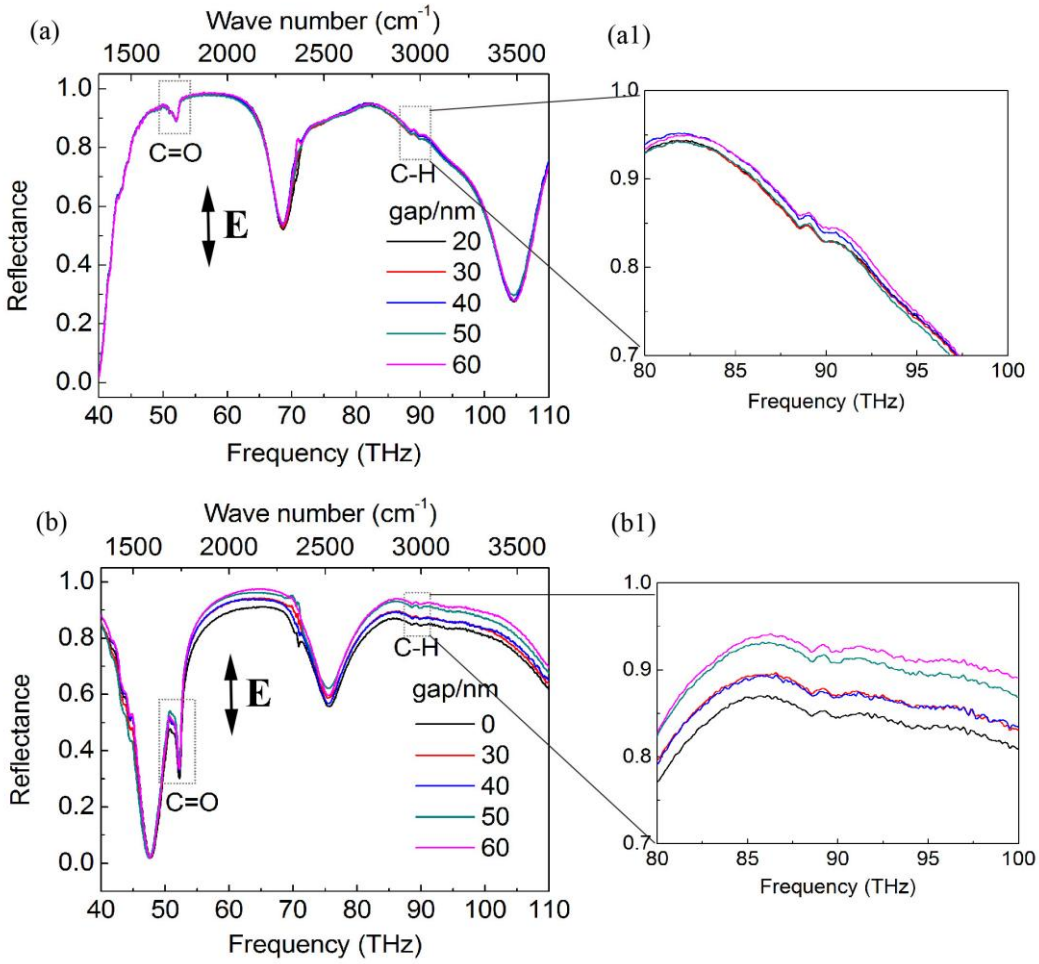

Figure 10. SEIRA spectroscopy of PMMA deposited on the pad-rod nanoantennas with y-polarized excitation

5. Conclusion

In conclusion, we have demonstrated dual and triple-resonant plasmonic nanoantnennas based on the MIM pad-rod structures. The combination of the large pad and nanotip with a reflective Au mirror can greatly enhance the local fields. Due to the charge squeezing from pad to tips, the local electric field in the gap is further boosted in comparison to traditional nanorod antennas. The numerically calculated EFs of SEIRA of the pad-rod antennas are around 1.8×10^{6}, which is the highest level of the reported nanoantennas for SEIRA. Molecular modes of C=O, C-H of PMMA were clearly identified with the plasmonic

antennas by SEIRA. These results demonstrate the potential of the pad-rod nanoantennas to work as effective sensing devices for single molecular detection.

Acknowledgement

This work is supported by CAS "Light of West China" Program and Sichuan Science and Technology Program (2018JY0616).

Notes and References:

[1] Ahmed A and Gordon R 2011 Directivity enhanced Raman spectroscopy using nanoantennas *Nano Lett.* **11** 1800–1803.

[2] Chirumamilla M, Toma A, Gopalakrishnan A, Das G, Zaccaria R P, Krahne R, Rondanina E, Leoncini M, Liberale C, Angelis F D and Fabrizio E D 2014 3d nanostar dimers with a sub-10-nm gap for single-/few-molecule surface-enhanced Raman scattering *Adv. Mater.* **26** 2353–2358.

[3] Huang J-A, Zhao Y-Q, Zhang X-J, He L-F, Wong T-L, Chui Y-S, Zhang W-J and Lee S-T, 2013 Ordered ag/si nanowires array: wide-range surface-enhanced Raman spectroscopy for reproducible biomolecule detection *Nano Lett.* **13** 5039−5045

[4] Yue W, Wang Z, Whittaker J, Lopez-royo F, Yang Y and Zayats A V 2017Amplification of surface-enhanced Raman scattering due to substrate-mediated localized surface plasmons in gold nanodimers *J. Mater. Chem. C* **5** 4075-4084

[5] Pryce I M, Kelaita Y A, Aydin K and Atwater H A 2011 Compliment metamaterials for resonantly enhanced infrared absorption spectroscopy and refractive index sensing *ACS Nano* **5** 8167–8174.

[6] Nishijima Y, Hashimoto Y, Rosa L, Khurgin J B and Juodkazis S 2014 Scaling rules of SERS intensity *Adv. Optical Mater.* **2** 382–388

[7] Yu Q, Guan P, Qin D, Golden G and Wallace P M 2008 Inverted size-dependence of surface-enhanced Raman scattering on gold nanohole and nanodisk arrays *Nano Lett.* **8** 1923-1928

[8] Cubukcu E, Zhang S, Park Y-S, Bartal G. and Zhang X 2009 Split ring resonator sensors for infrared detection of single molecular monolayers. *Appl. Phys. Lett.* 2009, 95, 043113.

[9] Baldassarre L, Sakat E, Frigerio J, Samarelli A, Gallacher K, Calandrini E, Isella G, Paul D J, Ortolani M and Biagioni P 2015 Midinfrared plasmon-enhanced spectroscopy with germanium antennas on silicon substrates *Nano Lett.* **15** 7225−7231

[10] Cerjan B, Yang X, Nordlander P and Halas N J 2016 Asymmetric aluminium antennas for self-calibrating surface-enhanced infrared absorption spectroscopy *ACS Photonics* **3** 354−360

[11] He X, Liu F, Lin F and Shi W 2019 Investigation of terahertz all-dielectric metamaterials *Opt. Express* **27** 13831-13844.

[12] He X, Xiao G, Liu F, Lin F and Shi W 2019 Flexible properties of THz graphene bowtie metamaterials structures *Opt. Mater. Express* **9** 44

[13] Shi C, He X, Peng J, Xiao G, Liu F, Lin F, Zhang H 2019 Tunable terahertz hybrid graphene-metal patterns metamaterials *Opt. Laser Technol.***114** 28–34

[14] Zhu W, Banaee M G, Wang D, Chu Y and Crozier K B 2011 Lithographically fabricated optical antennas with gaps well below 10 nm *Small* **7** 1761–1766

[15] Huck C, Neubrech F, Vogt J, Toma A, Gerbert D, Katzmann J, Härtling T and Pucci A 2014 Surface-enhanced infrared spectroscopy using nanometer-sized gaps *ACS Nano.* **8** 4908–4914

[16] Dodson S, Haggui M, Bachelot R, Plain J, Li S and Xiong Q 2013 Metamaterials-based label-free nanosensor for conformation and affinity biosensing *J. Phys. Chem. Lett.* **4** 496−501

[17] Aouani H, Rahmani M, Sipova H, Torres V, Hegnerova K, Beruete M, Homola J, Hong M, Navarro-Cia M and Maier S A 2013 Plasmonic nanoantennas for multispectral surface-enhanced spectroscopies *J. Phys. Chem. C* **117** 18620–18626

[18] Tao H, Landy N I, Bingham C M, Zhang X, Averitt R D and Padilla W J 2008 A metamaterial absorber for the terahertz regime: design, fabrication and characterization *Opt. Express* **16** 7181-7188

[19] He X, Liu F, Lin F, Xiao G and Shi W 2019 Tunable MoS2 modified hybrid surface plasmon waveguides. Nanotechnology **30** 125201

[20] Liu N, Mesch M, Weiss T, Hentschel M and Giessen H 2010 Infrared perfect absorber and its application as plasmonic sensor *Nano Lett.* **10** 2342–2348

[21] Bhattarai K, Ku Z, Silva S, Jeon J, Kim J O, Lee S J, Urbas A and Zhou J 2015 A large-area, mushroom-capped plasmonic perfect absorber: refractive index sensing and Fabry-Perot cavity mechanism *Adv. Optical Mater.* **3** 1779–1786

[22] Cetin A E, Korkmaz S, Durmaz H, Aslan E, Kaya S, Paiella R and Turkmen M 2016 Quantification of multiple molecular fingerprints by dual-resonant perfect absorber *Adv. Optical Mater.* DOI: 10.1002/adom.201600305

[23] Zhang N, Liu K, Liu Z, Song H, Zeng, Ji D, Cheney A, Jiang S and Gan Q 2015 Ultrabroadband metasurface for efficient light trapping and localization: a universal surface-enhanced Raman spectroscopy substrate for “all” excitation wavelengths *Adv. Mater. Interfaces* **2** 1500142.

[24] Chen K, Adato R and Altug H 2012 Dual-band perfect absorber for multispectral plasmon-enhanced infrared spectroscopy *ACS Nano* **6** 7998–8006

[25] Brown L V, Yang X, Zhao K, Zheng B Y, Nordlander P and Halas N J 2015 Fan-shaped gold nanoantennas above reflective substrates for surface-enhanced infrared absorption (SEIRA) *Nano Lett.* **15** 1272−1280

[26] Dong L, Yang X, Zhang C, Cerjan B, Zhou L, Tseng M L, Zhang Y, Alabastri A, Nordlander P and Halas N J 2017 Nanogapped Au antennas for ultrasensitive surface-enhanced infrared absorption spectroscopy *Nano Lett.* **17** 5768-5774

[27] CST website: https:// www.cst.com

[28] Liu X, Starr T, Starr A F and Padilla W J 2010 Infrared spatial and frequency selective metamaterial with near-unity absorbance *Phys. Rev. Lett.* **104** 207403

[29] Watts C M, Liu X and Padilla W J 2012 Metamaterial electromagnetic wave absorbers *Adv. Opt. Mater.* **24** OP98–OP120

[30] Liu N, Weiss T, Mesch M, Langguth L, Eigenthaler U, Hirscher M, Sönnichsen C and Giessen H 2010 *Nano Lett.* **10** 1103-1107

[31] Meinzer N, Barnes W L and Hooper I R 2014 Plasmonic meta-atoms and metasurfaces *Nature Photon.* **8** 889-898

[32] Pryce I M, Kelaita Y A, Aydin K and Atwate H A 2011 Compliant metamaterials for resonantly enhanced infrared absorption spectroscopy and refractive index sensing *ACS Nano* **5** 8167–8174

[33] Wei W, Nong J, Jiang X, Chen N, Luo S and Tang L 2017 All-semiconductor plasmonic resonator for surface-enhanced infrared absorption spectroscopy *micromachines* **8** 6